Transit Time of Lamb Wave-Based Ultrasonic Flow Meters and the Effect of Temperature

Daniel A. Kiefer , Andreas Benkert, and Stefan J. Rupitsch , *Member, IEEE*

Abstract—**Transit-time flow meters need to compensate for cross-sensitivity to temperature. We show that Lamb wave-based setups are less affected by temperature. An optimality criterion is derived that allows to tune the meter into a zero local sensitivity to temperature. For this end, the flow-induced change in ultrasonic transit time is revisited first. While wetted piston transducer meters are directly sensitive to the change in propagation speed, the change in time of flight of Lamb wave-based systems is due to the beam displacement. Second, the effect of temperature is incorporated analytically. It is found that the temperature-dependent radiation angle of Lamb waves is able to compensate for changes in the speed of sound, leading to an (almost) unaffected overall time of flight. This effect is achievable with any fluid and in a wide temperature range. As an example, we discuss a water meter in the range from 0 °C to 100 °C. The model is validated against temperature and flow rate-dependent measurements obtained on a prototype. The measured data fits well to the developed model and confirms the reduced cross-sensitivity to temperature. Although an in-line meter is considered here, the results extend to clamp-on devices.**

Index Terms—**Flow metering, leaky Lamb wave, noninvasive flowmeter, temperature, transit time, ultrasonic sensing.**

I. Introduction

ULTRASONIC flow meters (UFMs) measure the volumetric flow rate of a fluid through a pipe [1], [2]. Transit-time devices determine the flow rate based on the upstream-downstream difference in time of flight, which is due to ultrasonic convection in the flowing medium [3]. These popular kind of flow meters are available in a wide variety of designs. They fully play off their strengths when used in a noninvasive configuration, i.e., when the ultrasonic transducers are located outside the pipe. This leads to low-pressure drop, high robustness, and guarantees leak-tightness.

Daniel A. Kiefer was with the Chair of Sensor Technology, Friedrich-Alexander-Universität Erlangen-Nürnberg (FAU), 91052 Erlangen, Germany. He is now with the Institut Langevin, ESPCI Paris, Université PSL, CNRS, 75005 Paris, France (e-mail: daniel.kiefer@espci.fr).

Andreas Benkert is with Diehl Metering GmbH, 91522 Ansbach, Germany.

Stefan J. Rupitsch was with the Chair of Sensor Technology, Friedrich-Alexander-Universität Erlangen-Nürnberg (FAU), 91052 Erlangen, Germany. He is now with the Department of Microsystems Engineering, IMTEK, University of Freiburg, 79110 Freiburg, Germany.

The present contribution is concerned with a noninvasive inline flow meter that allows one to purposefully design the device's tube. Our findings are equally valid for clamp-on variants, i.e., systems that can be mounted onto existing piping installations.

The insonification of the pipe's interior is conventionally modeled using plane waves [1], [2], [4], [5], [6]. Thereby, the emitting ultrasonic transducer is assumed to generate a plane longitudinal wave inside a wedge that is clamped onto the pipe. This wave is then considered to convert to a pure transverse wave inside the pipe wall, which finally refracts into the fluid under certain angle θ out of the pipe wall's normal. This type of flow meter is referred to as a "shear mode device." The mentioned simple model is only valid above the first critical angle, i.e., for cutoff of the longitudinal wave inside the pipe wall. For water metering in a steel pipe, this restricts the irradiation angle to typically $15° \leq \theta \leq 28°$ [6].

The actual fluid angle θ will usually deviate from the angle predicted by the pure plane wave model, i.e., Snell's law. This is caused by the spatial filtering effect of the pipe wall (transfer function) acting on the finite aperture of the transducer (wide wavenumber spectrum) [4], [7], [8]. Note that inaccuracies in the fluid angle are detrimental because they lead to high errors in the measured flow rate [9]. Moreover, shear mode excitation leads to low transmission into the pipe's interior [2], [10]. Both effects are a consequence of driving the pipe wall outside its resonances.

An alternative approach considers that the transducer excites *guided waves* inside the pipe wall [6], [11]. These waves emerge due to superposition of transverse and longitudinal waves coupled through the pipe wall surfaces. They represent the generalized pipe wall resonances and are associated with the transmission maxima of the pipe wall [7], [8], [12]. Therefore, they are capable of efficiently insonifying the pipe's interior.

It is usually possible to idealize the pipe wall as an infinite plane plate and restrict to the waves having particle displacements solely in the cross-sectional plane of the plate. These solutions are denoted as *Lamb waves* [12], [13] and they are capable of radiating acoustic waves into the adjacent fluid—in which case they are denoted as *leaky Lamb waves* [14], [15]. In general, the Lamb waves propagate dispersively and multiple such modes are able to propagate, each with their own phase and group velocity. Although this makes the analysis more intricate, at the same time this provides more freedom for device design.

Flow meters that deliberately excite Lamb waves to insonify the pipe's interior shall be denoted as *Lamb wave-based UFMs*. They can be interpreted as a generalization to the so-called "wide-beam" flow meters that insonify the interior via continuous leakage [2], [16] (albeit the term is used differently in [8]). While wetted piston transducer or shear mode flow meters remain the most common and best studied systems, commercial meters exploiting Lamb waves are available on the market [16], [17], [18], [19] and are most often found in the context of clamp-on devices. A strength of Lamb wave-based UFMs is that they are less affected by axial misalignment of the transducers [7]. However, nonspecular reflection may result in distortion and shift of the reflected beam. The consequences for optimal transducer placement was examined by Aanes *et al.* [11]. Furthermore, the influence of pipe wall roughness, e.g., due to corrosion, was studied by Gu and Cegla [6].

The development of the flow profile $\mathbf{v}_0(x, y, z)$ inside the pipe is a hydrodynamic process of great importance in flow metering [1], [2], [5], [20]. Like any UFM, Lamb wave-based meters sense the mean velocity $\bar{v}_0$ of the fluid along the ray path. The explicit determination of the flow rate and the involved hydrodynamics are outside the scope of this contribution and we will, throughout, describe the ultrasonic convection in a mean acoustical sense by restricting to a homogeneous flow $\bar{v}_0$ in axial direction.

An ideal flow meter should be sensitive to the fluid flow rate only. In practice, however, the undesired cross-sensitivity to temperature plays a crucial role in any transit-time device. In fact, transit times are usually more affected by temperature-induced changes in the speed of sound c_f than by convection with the flow. Exploiting that with respect to the travel direction the two effects lead to equal and opposite transit-time changes, respectively, the upstream–downstream time of flight difference is less affected by temperature. Yet, for piston transducer devices it still exhibits a $1/c_f^2$-dependence on temperature [1], [2] and compensation remains the key for accurate measurements. The most common approach consists in using the average upstream–downstream time of flight to eliminate the dependence on the speed of sound in the flow equations [1], [2], [8], [11]. While differential time of flights are rather simple to acquire, this compensation mechanism additionally requires accurate measurements of the absolute time of flights, which can be very challenging.

The purpose of this contribution is twofold: 1) re-examine the convected ultrasonic time of flight in noninvasive flow meters and 2) analytically incorporate into this model the effect of temperature. Thereby, both the fluid as well as the pipe's response to temperature are accounted for. While point 1) may seem to be well studied, we remark that most publications on UFM start by assuming *changes in time of flight* due to an increased effective wave velocity in the flowing medium, which is not the case for noninvasive UFMs. This was recognized already in [5], [6], and [11]. A more detailed discussion and comparison between the two systems/models is provided here before incorporating temperature. To describe the effect of temperature on guided waves in the pipe wall, we derive a remarkably simple relation between changes in
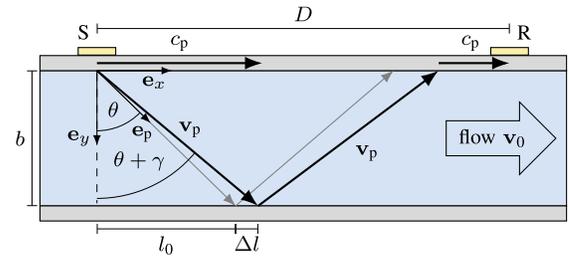

Fig. 1. Cross-sectional geometry of the Lamb wave-based flow meter. S: sender, R: receiver, c_p: phase velocity, θ: radiation angle, $\mathbf{e}_i$: directional vectors, $\mathbf{v}_0$: flow velocity, $\mathbf{v}_p$: convected ray velocity, γ: convection angle, Δl: convection distance, and l_0, b, and D: geometric dimensions as indicated.

the material parameters and the wave's phase velocity. The results presented in this article have been prepared in extended form for publication as a monograph [15], where some of the figures have been reprinted from.

The article is structured as follows: Section II introduces Lamb wave-based UFMs and derives the corresponding convected ultrasonic time-of-flight model. A comparison to the more conventional models used for wetted piston transducer meters is given in Section III. We incorporate the effect of temperature into the Lamb wave-based time of flight model in Section IV and the resulting consequences are analyzed. Lastly, Section V validates the developed model with flow and temperature-dependent measurements.

II. LAMB WAVE-BASED FLOW METER

The cross-sectional geometry of a Lamb wave-based UFM is sketched in Fig. 1. Two ultrasonic transducers that can either function as a sender (S) or as a receiver (R) are mounted on the pipe with an axial distance D. The sender generates a Lamb wave inside the pipe wall propagating with certain phase velocity c_p. Both the phase and group velocities of Lamb waves in an isotropic steel plate are shown for reference in Fig. 2, wherein each mode is labeled as symmetric (S) or antisymmetric (A). This computation can be performed with *GEW dispersion script* [21]. As the wave travels in axial direction, it radiates an inhomogeneous plane wave [14], [15], [22] into the fluid at an angle θ. It is a particularity of Lamb wave-based UFMs that the angle is given through $\theta = \arcsin c_f/c_p$, where c_f is the speed of sound of the fluid medium.[1] The radiated acoustic wave is reflected at the opposite pipe wall and then couples back into the upper pipe wall, where it is finally detected by the receiver (R). Note that in addition to this *V-path* signal going through the fluid, a *direct path* wave propagating exclusively in the pipe wall reaches the receiver.

A flowing medium *convects* sound leading to a change in propagation velocity as well as propagation direction [3]. This affects the overall time of flight from sender to receiver. The fact that convection breaks the reciprocity is usually exploited: while the downstream wave is accelerated, the upstream one is

---

[1]This expression for θ neglects the inhomogeneity of the radiated wave, i.e., the imaginary part of the wave vector in the fluid. It is valid for the lowly leaky waves associated with the propagating Lamb wave solutions shown in Fig. 2.
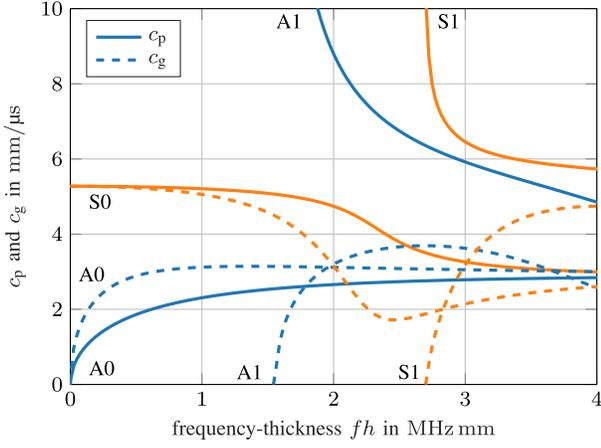
Fig. 2. Symmetric (S) and anti-symmetric (A) Lamb waves in an isotropic steel plate: the phase velocities c_p and group velocities c_g depend on the frequency-thickness product fh. Density: $\rho = 7900$ kg/m³, and Lamé parameters: $\lambda = 115$ GPa and $\mu = 76.9$ GPa.

slowed down. It is, hence, conventional and convenient to use the upstream–downstream differential time of flight $\tau^{\text{upstream}} - \tau^{\text{downstream}}$ to determine the flow velocity $\overline{v}_0$ and, ultimately, the flow rate Q. For this end, the role of sender and receiver are exchanged after the first measurement in order to obtain both the downstream as well as the upstream signal. This procedure removes all additive time delays due to reciprocal effects, i.e., those which are equal in both directions of propagation.

We define $\Delta\tau$ as the delay upstream with respect to zero flow when crossing the pipe once. For the V-path setup in Fig. 1 the total differential time of flight $\tau^{\text{upstream}} - \tau^{\text{downstream}}$ is hence $4\Delta\tau$ because the wave traverses the pipe twice in each direction. Figures throughout this article show representative quantities for the V-path meter and, hence, include the factor 4.

The time of flight τ from transducer to transducer, and in particular $\Delta\tau$, will be modeled in the following. Thereby, *ray tracing* [3] shall be used to include the effect of convection. A steady and homogeneous flow with velocity $\overline{v}_0$ is assumed. Using the radiation direction $\mathbf{e}_p = [\sin\theta, \cos\theta]^\top$ of the leaky Lamb wave, the ray velocity $\mathbf{v}_p$ at which the convected wave propagates is given by [3], [11]

$$\mathbf{v}_p = c_f\mathbf{e}_p + \overline{v}_0\mathbf{e}_x = c_f\begin{bmatrix}\sin\theta\\\cos\theta\end{bmatrix} + \begin{bmatrix}\overline{v}_0\\0\end{bmatrix}. \tag{1}$$

This leads to the transit time τ_f through the fluid, which reads

$$\tau_f = \frac{b}{\mathbf{v}_p \cdot \mathbf{e}_y} = \frac{b}{c_f\cos\theta} \tag{2}$$

and is found to be independent of the flow velocity $\overline{v}_0$. This was already noted in [11] and represents a big difference to conventional UFM with wetted piston transducers, as will be discussed in more detail in Section III.

Although the transit time through the fluid is independent of the flow velocity, the transit time from transducer to transducer is not. This is due to the flow-dependent location at which the wave couples back into the pipe wall. After traversing the pipe once, the beam is axially displaced by $\Delta l = [\mathbf{v}_p(\overline{v}_0) - \mathbf{v}_p(\overline{v}_0 = 0)] \cdot \mathbf{e}_x\tau_f$ with respect to zero flow. Using (1) and (2)
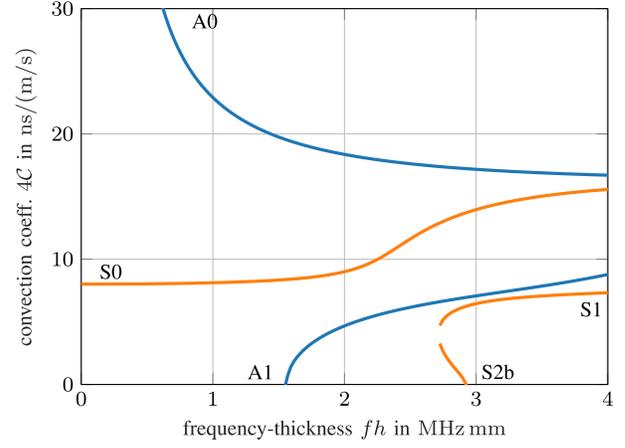

Fig. 3. Lamb wave-based UFM with a steel pipe: convection coefficients for water metering. Speed of sound: $c_f = 1480$ m/s and $b = 1.5$ cm.

results in

$$\Delta l = \overline{v}_0\tau_f = \frac{b}{c_f\cos\theta}\overline{v}_0. \tag{3}$$

This axial displacement of the convected ray corresponds to a change in arrival time $\Delta\tau$ seen by the receiver, namely

$$\Delta\tau = \frac{\Delta l}{c_p} = \mathcal{C}\overline{v}_0 \quad \text{with} \quad \mathcal{C} = \frac{b}{c_fc_p\cos\theta} \tag{4}$$

where we introduced the flow meter's *convection coefficient $\mathcal{C}$* for subsequent analysis. It describes the overall convective effect attained in the setup. The convection coefficient for water metering in a steel pipe is depicted in Fig. 3. From the above, we conclude that Lamb wave-based UFMs work analogous to conventional ranging systems: they are sensitive to the location of the source, in this case, the impinging V-path wave.

Lastly, for later reference, we derive the absolute time of flight τ. Using (2) as well as (3) and noting that the total distance traveled inside the pipe wall is $D - 2\,l_0 - 2\Delta l$ with $l_0 = b\tan\theta$, we obtain the absolute time of flight as

$$\tau = 2\tau_f + (D - 2\,l_0 - 2\Delta l)/c_p \tag{5a}$$

$$= \frac{D - 2\,b\tan\theta}{c_p} + 2\frac{b}{c_f\cos\theta}\left(1 - \frac{\overline{v}_0}{c_p}\right). \tag{5b}$$

Note that in contrast to $\Delta\tau$, τ depends on the transducer separation distance D.

The results derived above are a consequence of: 1) the oblique radiation from the pipe walls and 2) the fact that the radiating surfaces are aligned with the flow direction. These conditions and the derivations apply also to clamp-on UFMs. However, the working principle of UFMs with normally radiating piston transducers is different, as will be discussed in Section III.

III. COMPARISON TO NORMALLY RADIATING TRANSDUCER SETUPS

A UFM setup using wetted piston transducers is sketched in Fig. 4. The surface of such a transducer is designed to vibrate in phase everywhere and, thus, radiates acoustic waves
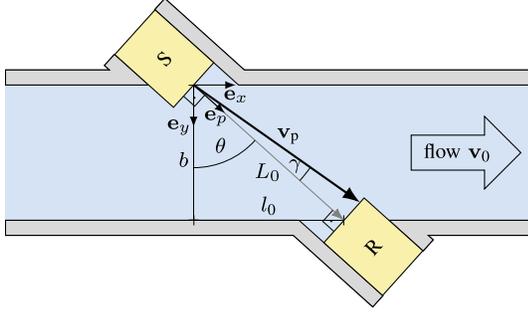
Fig. 4. Cross-sectional geometry of the wetted piston transducer-based flow meter. S: sender, R: receiver, θ: radiation angle, $\mathbf{e}_i$: directional vectors, $\mathbf{v}_0$: flow velocity, $\mathbf{v}_p$: convected ray velocity, γ: convection angle, and l_0, L_0, and b: geometric dimensions as indicated.
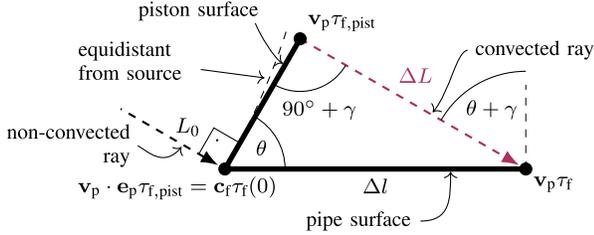

Fig. 5. Comparison of geometry of the two flow meters and the ray paths therein. The shown quantities are dependent on the mean flow velocity $\overline{v}_0$.

in normal direction. The radiating surface is no longer aligned with the fluid flow—as was the case for the Lamb wave-based UFM—but instead with the phase fronts of the emitted/received wave. Although convection in a homogeneous flow changes the propagation direction of the beam, it does not affect the orientation of the phase fronts [3]. This is, hence, an invariant of the design.

The transit time τ_f^{pist} through the fluid in Fig. 4 is different to the one for Lamb wave-based systems. In a very general manner, it is given by $\tau_f^{\text{pist}} = L^{\text{pist}}/|\mathbf{v}_p|$, where both the ray path length $L^{\text{pist}} = L_0/\cos(\gamma(\overline{v}_0))$ as well as the ray velocity $\mathbf{v}_p(\overline{v}_0)$ depend on flow velocity. Noting that $\cos\gamma = \mathbf{v}_p \cdot \mathbf{e}_p/|\mathbf{v}_p|$ and using (1) results in $L^{\text{pist}} = L_0|\mathbf{v}_p|/(c_f + \overline{v}_0 \sin\theta)$. This finally yields the sought transit time through the fluid as

$$\tau_f^{\text{pist}} = \frac{L_0}{c_f + \overline{v}_0 \sin\theta} \tag{6}$$

which is at the same time the transducer-to-transducer transit time τ^{pist}. In contrast to the Lamb wave-based UFM, it is directly dependent on the flow velocity $\overline{v}_0$.

The different transit times through the fluid of the two setups given in (2) and (6) can be explained by taking a closer look at the geometry and the ray paths. The situation in the region where the wave impinges at the bottom pipe wall (Lamb wave setup) or transducer (piston transducer setup) is shown in superposition in Fig. 5.

For a Lamb wave-based system, the path length changes considerably due to convection. Using (1), (2), and (6), we see

that the increase is

$$\Delta L = |\mathbf{v}_p|(\tau_f - \tau_f^{\text{pist}}) = \frac{\overline{v}_0}{c_f} b \frac{\tan\theta}{\cos\gamma} \approx \frac{\overline{v}_0}{c_f} b \tan\theta \tag{7}$$

with respect to the almost constant piston transducer ray path length of $|\mathbf{v}_p|\tau_f^{\text{pist}} = L = L_0/\cos\gamma \approx L_0$. The approximations hold for small convection angles γ. This reveals that the metering effect of Lamb wave-based devices is fundamentally different to piston transducer meters: the former is based on a *change in travel distance*, while the latter is due to a *change in the ray velocity*.

Similar as for the Lamb wave-based setup, the piston transducer flow meters actually acquire the differential time of flight rather than the absolute one. With respect to zero-flow condition, it can be obtained from the overall transit time (6) as $\Delta\tau^{\text{pist}} = \tau_f^{\text{pist}}(\overline{v}_0) - \tau_f^{\text{pist}}(\overline{v}_0 = 0)$ and simplifies to

$$\Delta\tau^{\text{pist}} = b \tan\theta \frac{\overline{v}_0}{c_f^2 - \overline{v}_0^2 \sin^2\theta}. \tag{8}$$

The two effects described by (8) and (4) are similar in magnitude, the relative difference being

$$\frac{\Delta\tau^{\text{pist}} - \Delta\tau}{\Delta\tau} = \frac{\overline{v}_0^2}{c_p^2 - \overline{v}_0^2} \approx \left(\frac{\overline{v}_0}{c_p}\right)^2. \tag{9}$$

As flow meters operate at low Mach numbers, i.e., $\overline{v}_0 \ll c_f$, the two effects are indeed very similar in practice. Note, however, that the origins for the change in time of flight are in fact different ones, as was explained above.

A short discussion on how the commonly used "effective wave speed" approach relates to the above ray tracing models is in order. The well-known results shown in (6) and (8) are usually obtained by projecting the ray velocity $\mathbf{v}_p$ onto the original propagation direction $\mathbf{e}_p$ [6]. This results in an "effective wave speed" of $c_f + \overline{v}_0 \sin\theta$ along the zero-flow path [1], [2]. For the piston transducers, the "effective wave speed" formalism and the ray-tracing approach yield identical results. This is due to the *wavefront being aligned with the transducer surface* and arriving everywhere at the same time. Accordingly, it does not matter which particular point on the phase front is traced, i.e., the considered wave path is irrelevant and a projection can be done.

On the other hand, the effective wave speed cannot, strictly speaking, be used with a Lamb wave-based setup. The convected ray's projection onto its zero-flow path is compared to the actual ray in Fig. 6. When the convected ray reaches the point P, the projected ray will be at l_0 and then propagates with the phase velocity $c_p = c_f/\sin\theta$ to the target point $l_0 + \Delta l$. Contrary to this, the convected ray propagates with the convected tracing velocity of $c_f/\sin\theta + \overline{v}_0$ all the way to $l_0 + \Delta l$, arriving slightly earlier than its projected counterpart. This explains the difference between the differential time of flights in (8) and (4).

We conclude that for the obliquely radiating Lamb wave-based setup, the ray-tracing model according to (2) and (4) is the accurate one, represents the actual physics and should be used for further modeling. Particularly important is the explicit dependence on c_p, which will be exploited in the next section to analyze the effect of temperature.
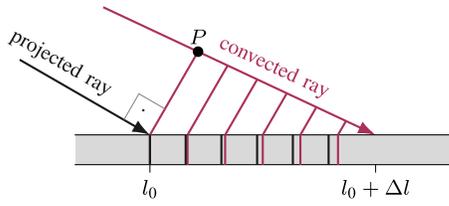
Fig. 6. Projected versus convected ray: the latter arrives earlier at $l_0 + \Delta l$ as it is convected longer.
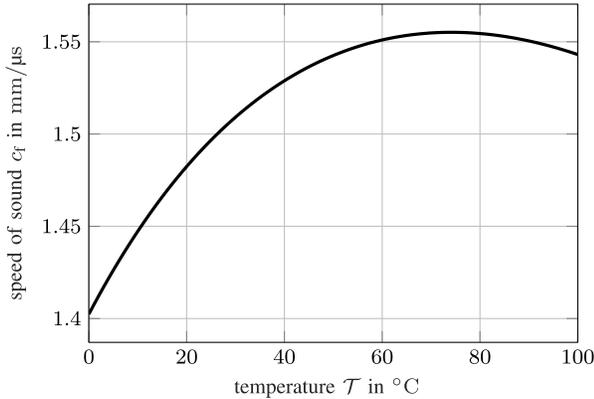

Fig. 7. Speed of sound in water in dependence of temperature according to [23].

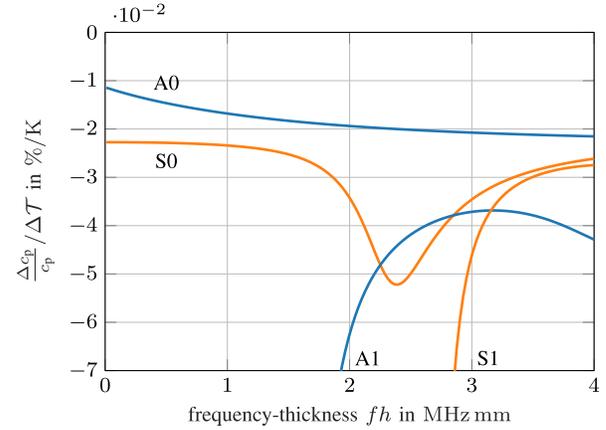Fig. 8. Lamb waves in steel: relative change in phase velocity per unit change in temperature with respect to 20 °C.

IV. TEMPERATURE EFFECT

In the following, the temperature dependence shall be incorporated into the model given by (4) in an analytical manner. Temperature acts on the system in two different ways: 1) changing the wave propagation in the pipe, i.e., c_p and 2) affecting the speed of sound of the fluid, i.e., c_f. The speed of sound c_f will be modeled by a polynomial fit to measured data as provided by Bilaniuk and Wong [23], [24]. It is plotted for later discussion in Fig. 7. On the other hand, the effect 1) that acts on the pipe wall requires a detailed analysis of Lamb wave propagation and will be presented next.

A. Effect on the Pipe Wall

As Lamb waves propagate dispersively, a mode and frequency-dependent analysis of their phase velocities $c_p(\mathcal{T})$ is called for. We use perturbation of the initial solutions at reference temperature to obtain a simple analytical expression.

For this end, consider a Lamb wave that propagates in a plate with through-thickness coordinate $y \in [-h/2, h/2]$. It has an associated strain field $\mathbf{S}$ and carries the power $\overline{P}$. According to [13], a change of $\Delta \mathbf{c}$ in the stiffness tensor will lead to a relative change in phase velocity of

$$\frac{\Delta c_p}{c_p} = \frac{c_p}{4\overline{P}} \int_{-h/2}^{h/2} \mathbf{S}^* : \Delta \mathbf{c} : \mathbf{S} \, dy \qquad (10)$$

where $\bullet^*$ denotes complex conjugation.

A change $\Delta \mathcal{T}$ in temperature with respect to the reference $\mathcal{T}_0$ leads to a corresponding perturbation ΔE of the Young's modulus E of the isotropic material. The effect is linear in good approximation, such that $\Delta E = E' \Delta \mathcal{T}$, wherein E' represents the *temperature coefficient* characterizing the material. Moreover, the stiffness can be factorized as $\mathbf{c} = E\mathbf{N}$, where the fourth-order tensor $\mathbf{N}$ depends only on the Poisson's ratio. The impact of changes in the latter is typically about one order of magnitude below that of E [15] and we assume $\mathbf{N}$ constant in the following. Exploiting these circumstances to set $\Delta \mathbf{c} = \Delta E\mathbf{N} = (\Delta E / E)\mathbf{c}$, the ratio $\Delta E/E$ can be factored out of the integral to yield

$$\frac{\Delta c_p(\mathcal{T})}{c_p} = \frac{E'}{E} \frac{c_p}{4\overline{P}} \Delta \mathcal{T} \int_{-h/2}^{h/2} \mathbf{S}^* : \mathbf{c} : \mathbf{S} \, dy. \qquad (11)$$

Therein, all quantities are taken at reference temperature unless otherwise indicated. Due to equipartition of kinetic and elastic energy [13], [25], the integral is identified as twice the total stored energy $\overline{H}$. The ratio $\overline{P}/\overline{H}$ defines the *energy velocity*, which is equal to the *group velocity* c_g [13], [25]. This leads to a simple expression for the relative change in phase velocity, namely

$$\frac{\Delta c_p(\mathcal{T})}{c_p} = \frac{1}{2} \frac{c_p}{c_g} \frac{E'}{E} \Delta \mathcal{T}. \qquad (12)$$

Note that (12) can be evaluated without explicitly determining the Lamb wave strain field $\mathbf{S}$ because c_g relates to the phase velocity by $c_g = c_p[1 - (f/c_p)(\partial c_p/\partial f)]^{-1}$, where f denotes the frequency [26].

The resulting relative changes in phase velocity per unit change in temperature in a steel plate are depicted in Fig. 8. Albeit the effect is relatively small, the large temperature range on which flow meters are operated lead to relevant changes in phase velocity. We remark that metals exhibit negative temperature coefficients. Consequently, the phase velocity decreases with temperature—except for backward waves, which have negative c_p/c_g [13], e.g., the wave marked S2b in Fig. 3.

B. Overall Temperature Model

The relation $\sin \theta = c_f/c_p$ can be used to eliminate either θ or c_p from (4). In doing so, we obtain the

two representations[2]

$$\mathcal{C}(\mathcal{T}) = \frac{b}{c_{\mathrm{f}}(\mathcal{T})\sqrt{c_{\mathrm{p}}^2(\mathcal{T}) - c_{\mathrm{f}}^2(\mathcal{T})}} \tag{13a}$$

$$= \frac{b \tan \theta(\mathcal{T})}{c_{\mathrm{f}}^2(\mathcal{T})} \tag{13b}$$

where the temperature dependence is indicated. The first form given in (13a) is particularly suited for Lamb wave-based devices, as it clearly separates the fluid and pipe domains into c_{f} and c_{p}, respectively. Their respective behavior with temperature was discussed previously, hence, we have obtained the full flow meter model accounting for temperature.

C. Discussion of the Effect of Temperature

For reference in the further discussion, we note that the temperature behavior of piston transducer meters is described by (13b) with a fixed radiation angle, i.e., setting $\theta(\mathcal{T}) = \theta_0$. This leads to the well-known square dependence on the speed of sound [1], [2], and accordingly to large variations in the acquired differential time of flight. The differential relative change in $\mathcal{C}$ per unit $\Delta\mathcal{T}$ is given by $(\partial\mathcal{C}/\partial\mathcal{T})/\mathcal{C} = -2c_{\mathrm{f}}'/c_{\mathrm{f}}$, where $\bullet' = \partial\bullet/\partial\mathcal{T}$. Note that it depends only on the fluid medium and the cross-sensitivity to temperature must, therefore, be compensated *a posteriori*.

This is different for Lamb wave-based UFM, as can be seen in (13a) by inspecting the temperature dependence of $c_{\mathrm{f}}(\mathcal{T})$ and the square root. While one of them increases, the other one will usually decrease, leading to smaller variations in $\mathcal{C}(\mathcal{T})$ and, hence, also in $\Delta\tau(\mathcal{T})$. Let us assume for a moment that c_{p} is constant. The opposite behavior of the two terms is then due to the negative sign of c_{f} in the square root. It is remarkable that it is irrelevant whether c_{f} increases or decreases with temperature. As a result, this behavior is universal in that it can be observed in any fluid medium. From a physical point of view, this compensation effect can be ascribed to the changing radiation angle of leaky Lamb waves according to (13b), where $\tan\theta(\mathcal{T})$ may (partially) compensate $c_{\mathrm{f}}^2(\mathcal{T})$. We emphasize again that the radiation angles will change even when c_{p} is constant. For the case of water metering in a metallic pipe, c_{f} is mostly increasing while c_{p} decreases, leading to an even stronger temperature compensation as will be discuss in more detail later on.

For more insight, let us inspect the differential relative change with respect to temperature, given by

$$\frac{1}{\mathcal{C}}\frac{\partial\mathcal{C}}{\partial\mathcal{T}} = \frac{c_{\mathrm{f}}'\left(2c_{\mathrm{f}}^2 - c_{\mathrm{p}}^2\right) - c_{\mathrm{p}}'c_{\mathrm{p}}c_{\mathrm{f}}}{c_{\mathrm{f}}\left(c_{\mathrm{p}}^2 - c_{\mathrm{f}}^2\right)}. \tag{14}$$

In accordance with the previous discussion, even for $c_{\mathrm{p}}' = 0$ (no effect on the pipe), we can find an optimal operating point, namely $c_{\mathrm{p}}^* = \sqrt{2}c_{\mathrm{f}}$, where the meter is locally insensitive to temperature. More generally, $c_{\mathrm{p}}' \approx \Delta c_{\mathrm{p}}/\Delta\mathcal{T}$ is given by (12). Inserting into (14) yields the *optimality criterion*

$$c_{\mathrm{f}}'\left(2c_{\mathrm{f}}^2 - c_{\mathrm{p}}^2\right) - \frac{1}{2}\frac{c_{\mathrm{p}}^3}{c_{\mathrm{g}}}\frac{E'}{E}c_{\mathrm{f}} = 0. \tag{15}$$

[2]Note that $\cos\arcsin(c_{\mathrm{f}}/c_{\mathrm{p}}) = \sqrt{1 - c_{\mathrm{f}}^2/c_{\mathrm{p}}^2}$.
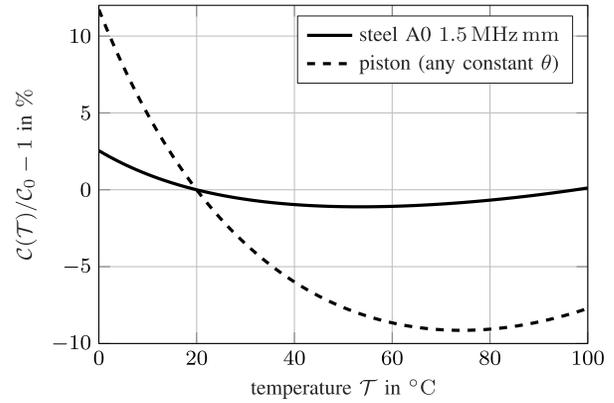

Fig. 9. Relative change with temperature of the convection coefficients $\mathcal{C}$ of a Lamb wave-based flow meter compared to a conventional piston transducer device. The different behavior is due to the temperature-dependent radiation angle θ of Lamb wave-based meters.

It allows us to choose a combination of material (E'/E) and operating point $(c_{\mathrm{p}}, c_{\mathrm{g}})$ that exhibits zero cross-sensitivity to temperature. Note moreover that, if desired, the operating point can be adjusted during operation by exploiting its frequency dependence. This could enable one to counteract, e.g., the nonlinearity in $c_{\mathrm{f}}(\mathcal{T})$ or aging effects.

The previous discussion focused on the behavior close to some reference temperature. Flow meters must usually be operational in a wide temperature range, which requires to account for the nonlinear temperature dependence $c_{\mathrm{f}}(\mathcal{T})$, see Fig. 7. The impact of temperature on the range $\mathcal{T} \in [0\,°\mathrm{C}, 100\,°\mathrm{C}]$ is shown in Fig. 9 for a Lamb wave-based system in comparison to a piston transducer setup. The lower sensitivity to temperature of the Lamb wave-based meter close to $\mathcal{T}_0 = 20\,°\mathrm{C}$ is immediately evident by inspecting the corresponding slope. Note that the same holds for almost all other values of temperature. Consequently, one observes smaller variations of $\mathcal{C}(\mathcal{T})$ on the entire temperature range.

Each operating point (c_{p}, f) leads to a different convection coefficient $\mathcal{C}(\mathcal{T})$ and corresponding variation with temperature. In order to systematically quantify the overall effect of temperature for different devices, the global root-mean-square relative variation due to temperature is defined as

$$F_{\mathrm{rel}} \overset{\mathrm{def}}{=} \frac{1}{\mathcal{C}_0}\left(\frac{1}{100\,°\mathrm{C}}\int_{0\,°\mathrm{C}}^{100\,°\mathrm{C}}(\mathcal{C}(\mathcal{T}) - \mathcal{C}_0)^2\,\mathrm{d}\mathcal{T}\right)^{1/2} \tag{16}$$

where $\mathcal{C}_0 = \mathcal{C}(\mathcal{T}_0)$. This represents, hence, the root-mean-square of the curves in Fig. 9. A small variation F_{rel} is desirable, as it indicates that the meter's behavior does barely change on the inspected temperature range. The resulting mode and frequency-dependent F_{rel} for a steel pipe are presented in Fig. 10.

Albeit this passive temperature compensation effect does not allow to attain a zero global temperature variation of the convection coefficient, the minimum lies at about 0.5% when using the $A0$ wave, which compares to 7.8% for piston transducer flow meters. It is remarkable that almost any choice of operating point leads to a reduced cross-sensitivity to temperature compared to piston transducers. Even materials
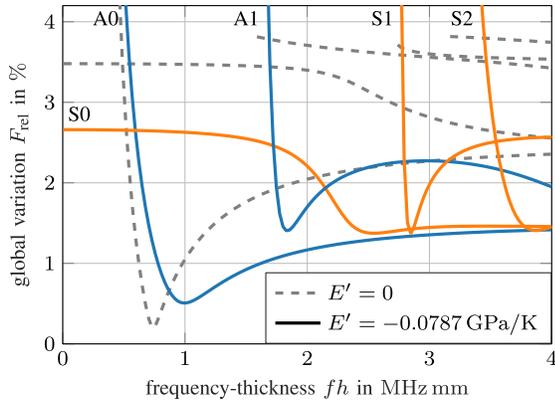
Fig. 10. Global root-mean-square relative variation F_{rel} of the meter's convection coefficient $\mathcal{C}$ due to temperature as defined in (16). A steel pipe with temperature-dependent Young's modulus (solid lines) is compared to the case where constant phase velocities are assumed (dashed lines). For piston transducer meters, the corresponding temperature variation is $F_{rel} = 7.8\%$.
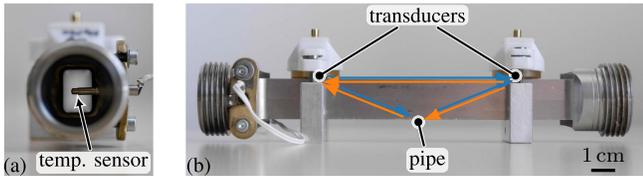

Fig. 11. Prototype in (a) front view and (b) lateral view. The transducers send alternately upstream (blue) and downstream (orange). The temperature sensor serves as reference only.

Fig. 12. Example of recorded ultrasonic upstream and a downstream signals at 6021 L/h and 19.9 °C.

with $E' = 0$, i.e., assuming constant phase velocities, exhibit relatively small variations in $\mathcal{C}(\mathcal{T})$. The negative temperature coefficient E' of metals helps to further reduce F_{rel}.

Overall, it may be concluded that Lamb wave-based flow meters exhibit significantly reduced cross-sensitivity to temperature when compared to classical piston transducer setups. The effect is universal in that it can potentially be observed in any fluid medium and pipe. However, the final effectiveness quite strongly depends on the pipe's temperature-behavior $c_p(\mathcal{T})$ and the chosen operating point (mode and frequency) and can help to further reduce this cross-sensitivity. The effect as well as the developed flow meter model will be validated in the sequel.

V. MEASUREMENTS AND VALIDATION

A prototype was fabricated consisting of a 1.5 mm thick rectangular steel pipe and is depicted in Fig. 11. Its inner dimensions are $b = 15$ mm and $d = 10$ mm (see Fig. 1). The ultrasonic comb array transducers are separated by $D = 9$ cm and excite an A0 Lamb wave pulse centered at 1 MHz. The received signal consists of a direct wave and a V-path pulse. An example of recorded upstream and downstream signals is shown in Fig. 12 together with their instantaneous phase difference obtained from their Hilbert transforms.

A set of 7665 measurements under controlled flow and temperature conditions was obtained at the test facility of Diehl Metering GmbH, Ansbach, Germany. The target nominal values for the flow rate in L/h were 6.4, 63, 630, 4000,
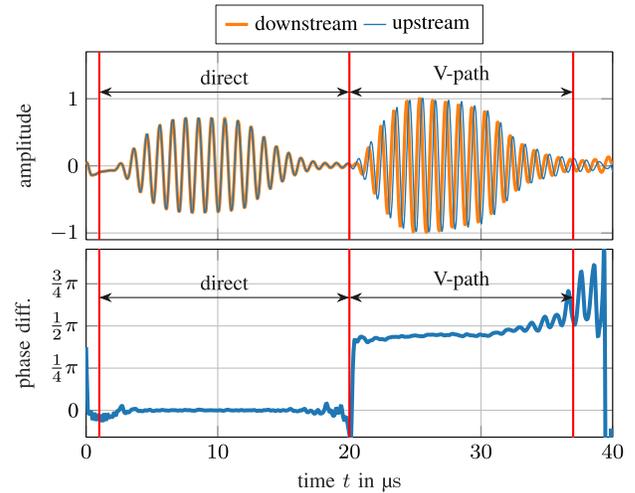
5000, and 6000; the ones for temperature were from 10 °C to 90 °C in steps of 10 °C. The mean flow velocity will be assumed throughout as $\bar{v}_0 \approx Q/(bd)$, i.e., as an approximation to the turbulent flow regime ($Q \gtrsim 1200$ L/h). Each measurement consists of upstream and downstream recorded ultrasonic signals similar to Fig. 12. Moreover, reference measurements were obtained for the volumetric flow rate (Q_{ref}) as well as the temperature ($\mathcal{T}_{ref}$).

The phase of the V-path pulse is evaluated systematically by reading out the phase of the Fourier transform at 1 MHz. Evaluating only downstream signals and unwrapping the obtained phase leads to the absolute downstream time of flight presented in Fig. 13(a). The experimental data coincide well with the model according to (5b), where the temperature dependence of $c_f(\mathcal{T})$, $c_p(\mathcal{T})$, and $\theta(c_p, c_f)$ has been considered according to Section IV. Thereby, the temperature coefficient E' of the Young's modulus was adjusted to minimize the errors and yields -0.0993 GPa/K, compared to -0.0787 GPa/K expected from the material datasheet.

The measured upstream–downstream differential time of flight is obtained in a similar fashion and is presented in Fig. 13(b). The model $4\Delta\tau = 4\mathcal{C}(\mathcal{T})\bar{v}_0$ according to (13a) is also shown. The data points lie again well within the model surface. The expected behavior of a corresponding piston transducer device is superposed for comparison and is seen to exhibit larger temperature variations.

For a more quantitative assessment inspect Fig. 14, which shows the convection coefficient $\mathcal{C}(\mathcal{T}) = \Delta\tau/\bar{v}_0$ as determined from the measurement data in comparison to the models. Thereby, only the turbulent flow regime is taken into account because in this case, the hydrodynamic correction factor tends toward unity and can be neglected. The measurements clearly follow the trend of the proposed model. The standard variations range from 0.12 to 0.26 ns/(m s⁻¹) and are believed to be mainly due to imprecise knowledge of the true flow rate. Note that while the reference temperature is measured with a dedicated sensor inside the device, the reference flow rate is obtained as a mean from the flow controller. In particular, the
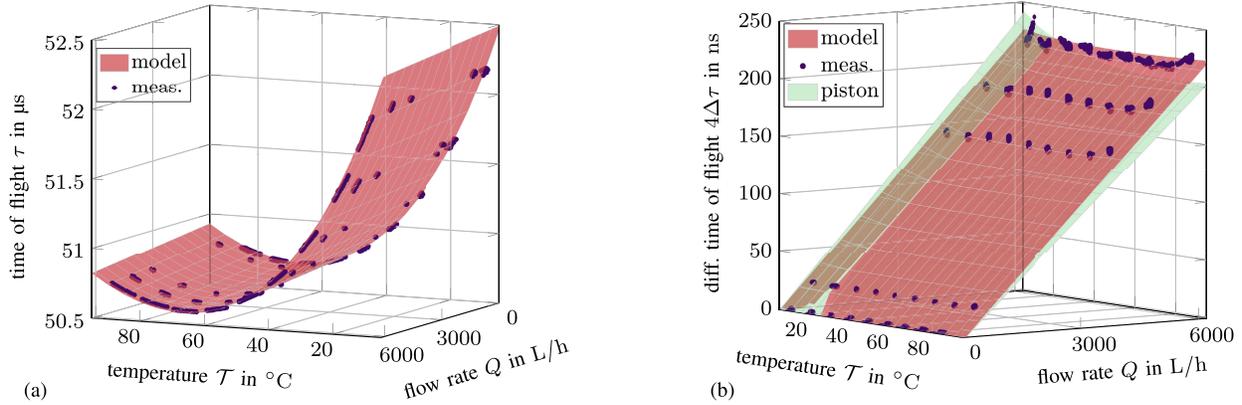
Fig. 13. Measurement compared to the model: the acquired (a) absolute and (b) differential time of flights match well with the temperature and flow rate-dependent model developed for Lamb wave-based flow meters. The corresponding behavior of piston transducer setups is also shown in (b) and expects a considerably larger variation with temperature.
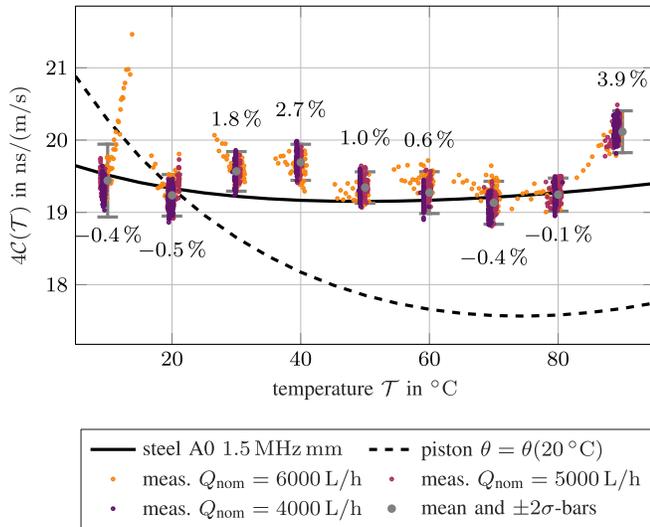

Fig. 14. Measured flow meter's convection coefficients $\mathcal{C}(\mathcal{T})$ in the turbulent regime compared to the model. The relative deviation to the model is indicated. The Lamb wave-based meter model is compared to the behavior expected for a conventional piston transducer device.

measurement at low temperature and high flow rate exhibits a systematic deviation, which we suspect to be caused by an unsteady valve position of the flow controller. Moreover, while the temperature of the water source is controlled, the device's temperature itself is not. This leads to unaccounted-for temperature gradients and unsteadiness through the system and according deviations to the model.

In view of the discussed uncertainties in the measurement setup, the obtained data lies overwhelmingly close to the proposed model. This confirms that the measurement data cannot be explained by assuming a temperature-independent radiation angle (i.e., piston transducer). Concluding we may state that the reduced cross-sensitivity to temperature of the Lamb wave-based UFM is clearly observable.

VI. CONCLUSION

Ultrasonic convection due to fluid flow leads to a change in transducer-to-transducer time of flight. We showed that,

in principle, the nature of this effect is a different one for Lamb wave-based UFMs than for classical piston transducer UFMs—albeit both effects are very similar in magnitude.

Starting from the natural time-of-flight model for Lamb wave-based UFMs, the effect of temperature has been included in an analytical manner. We find that these UFMs exhibit significantly lower cross-sensitivity to temperature as compared to classical setups. The effect can be tuned via the pipe material's temperature coefficient and choice of the Lamb wave mode and frequency. Although zero variation of the device's convection coefficient in a wide temperature range is not achievable for water flow metering, a local zero-cross-sensitivity is feasible. The effect of the discussed intrinsic compensation to temperature was confirmed by measurements on a UFM prototype under controlled temperature and flow rate.

The herein considered rectangular pipe for the inline flow meter cannot always be adopted. In particular, clamp-on flow meters rely on cylindrical pipes. We remark that the developed model extends to the cylindrical case. For the sake of accuracy, the calculations could then be done with guided waves in cylinders. However, for usual pipe dimensions, the Lamb wave solutions are very good approximations to the thin-walled cylinders and could in most cases still be used without significant deviations in the model.

This study focused solely on the ultrasonic behavior of the system. To obtain a more accurate model, the hydrodynamics should be included which leads to an additional temperature and flow dependence. Moreover, it was assumed that the fluid and the pipe are at a uniform temperature. The model could further be improved by including the actual heat dynamics. Note that not only the environment's temperature will be of relevance, but the flowing medium can also lead to fast changes of temperature in the entire system.

Lastly, we remark that Lamb waves form a complete bi-orthogonal set that is able to fully describe the pipe wall mechanics [13]. As a consequence, modeling flow meters with Lamb waves is a very general approach and could be regarded as an alternative modeling method rather than a specific kind of device.

REFERENCES

[1] S. J. Rupitsch, *Piezoelectric Sensors and Actuators—Fundamentals and Applications* (Topics in Mining, Metallurgy and Materials Engineering). Berlin, Germany: Springer, Aug. 2018.

[2] O. Fiedler, *Strömungs- und Durchflussmesstechnik (Current and Flow Measurement Technology)*. München, Germany: Oldenbourg: Industrieverlag, 1992.

[3] A. D. Pierce, *Acoustics: An Introduction to its Physical Principles and Applications*, 3rd ed. Woodbury, NY, USA: Acoustical Society of America, 1994.

[4] P. Ploss, "Untersuchung von Clamp-on-Ultraschalldurchflussmessgeräten im k-Raum (Study of clamp-on ultrasonic flow meters in k-space)," Doctoral dissertation, FAU Erlangen-Nürnberg, Erlangen, Germany, 2016.

[5] O. Keitmann-Curdes and B. Funck, "A new calibration method for ultrasonic clamp-on transducers," in *Proc. IEEE Ultrason. Symp.*, Nov. 2008, pp. 517–520, doi: 10.1109/ULTSYM.2008.0125.

[6] X. Gu and F. Cegla, "Modeling surface roughness-related uncertainties of leaky Lamb wave clamp-on ultrasonic flowmeters," *IEEE Trans. Instrum. Meas.*, vol. 69, no. 9, pp. 6843–6852, Sep. 2020, doi: 10.1109/TIM.2020.2975389.

[7] B. Funck and A. Mitzkus, "Acoustic transfer function of the clamp-on flowmeter," *IEEE Trans. Ultrason., Ferroelectr., Freq. Control*, vol. 43, no. 4, pp. 569–575, Jul. 1996, doi: 10.1109/58.503717.

[8] R. Motegi, S. Takeuchi, and T. Sato, "Widebeam ultrasonic flowmeter," in *Proc. IEEE Symp. Ultrason.*, vol. 1, Dec. 1990, pp. 331–336, doi: 10.1109/ULTSYM.1990.171380.

[9] P. Ploss, S. J. Rupitsch, and R. Lerch, "Extraction of spatial ultrasonic wave packet features by exploiting a modified Hough transform," *IEEE Sensors J.*, vol. 14, no. 7, pp. 2389–2395, Jul. 2014, doi: 10.1109/JSEN.2014.2311160.

[10] A. Luca, R. Marchiano, and J.-C. Chassaing, "Numerical simulation of transit-time ultrasonic flowmeters by a direct approach," *IEEE Trans. Ultrason., Ferroelectr., Freq. Control*, vol. 63, no. 6, pp. 886–897, Jun. 2016, doi: 10.1109/TUFFC.2016.2545714.

[11] M. Aanes, R. A. Kippersund, K. D. Lohne, K.-E. Frøysa, and P. Lunde, "Time-of-flight dependency on transducer separation distance in a reflective-path guided-wave ultrasonic flow meter at zero flow conditions," *J. Acoust. Soc. Amer.*, vol. 142, no. 2, pp. 825–837, Aug. 2017, doi: 10.1121/1.4996851.

[12] D. Royer and T. Valier-Brasier, *Ondes Élastiques Dans les Solides 1: Propagation (Elastic Waves in Solids 1: Propagation)* (Collection Ondes), vol. 1. London, U.K.: ISTE éditions, 2021.

[13] B. A. Auld, *Acoustic Fields and Waves in Solids*, vol. 2, 2nd ed. Malabar, FL, USA: Krieger Publishing Company, 1990.

[14] D. A. Kiefer, M. Ponschab, S. J. Rupitsch, and M. Mayle, "Calculating the full leaky Lamb wave spectrum with exact fluid interaction," *J. Acoust. Soc. Amer.*, vol. 145, no. 6, pp. 3341–3350, Jun. 2019, doi: 10.1121/1.5109399.

[15] D. A. Kiefer, *Elastodynamic Quasi-Guided Waves for Transit-Time Ultrasonic Flow Metering* (FAU Forschungen, Reihe B, Medizin, Naturwissenschaft, Technik), vol. 42, Erlangen, Germany: FAU Univ. Press, 2022, doi: 10.25593/978-3-96147-550-6.

[16] J. Doorhy. (Sep. 2011). *Strength in Numbers: Matching Lamb Wave Sensors to the Resonant Frequency of a Pipe Wall.* [Online]. Available: https://cache.industry.siemens.com/dl/files/254/109766254/att_980609/v1/SensorChoices.pdf

[17] B. Koenig, Y. Hoog, C. Gittinger, and Y. Fuchs, "Device for determining properties of a medium," U.S. Patent 9 581 572 B2, Feb. 28, 2017.

[18] E. Twerdowski and C. Heinks, "Acoustic flowmeter and method for non-invasively determining the flow of a medium in an electrically conducting object," U.S. Patent 9 664 543 B2, May 30, 2017.

[19] R. A. Kippersund, K. E. Frøysa, and P. Lunde, "Flow measuring apparatus," U.S. Patent 8 141 434 B2, Mar. 27, 2012.

[20] P. I. Moore, G. J. Brown, and B. P. Stimpson, "Ultrasonic transit-time flowmeters modelled with theoretical velocity profiles: Methodology," *Meas. Sci. Technol.*, vol. 11, no. 12, pp. 1802–1811, Dec. 2000, doi: 10.1088/0957-0233/11/12/321.

[21] D. A. Kiefer. (Aug. 19, 2022). *GEW Dispersion Script*, doi: 10.5281/zenodo.7010603.

[22] E. M. Viggen and H. K. Arnestad, "Understanding sound radiation from surface vibrations moving at subsonic speeds," in *Proc. 44th Scand. Symp. Phys. Acoust.*, Feb. 2021, pp. 1–4.

[23] N. Bilaniuk and G. K. Wong, "Speed of sound in pure water as a function of temperature," *J. Acoust. Soc. Amer.*, vol. 93, no. 3, pp. 1609–1612, Mar. 1993, doi: 10.1121/1.406819.

[24] N. Bilaniuk and G. K. Wong, "Erratum: Speed of sound in pure water as a function of temperature," *The J. Acoust. Soc. Amer.*, vol. 99, no. 5, p. 3257, May 1996, doi: 10.1121/1.415224.

[25] K.-J. Langenberg, R. Marklein, and K. Mayer, *Ultrasonic Nondestructive Testing of Materials: Theoretical Foundations*, 1st ed. Boca Raton, FL, USA: CRC Press, Feb. 2012.

[26] J. D. Achenbach, *Wave Propagation in Elastic Solids*. Amsterdam, The Netherlands: North Holland, Nov. 1987.